Res Chem Intermed (2015) 41:6649–6664
DOI 10.1007/s11164-014-1767-6

Luminescence properties of Eu^{2+}, Dy^{3+}-doped $Sr_2MgSi_2O_7$, and $Ca_2MgSi_2O_7$ phosphors by solid-state reaction method

Ishwar Prasad Sahu · D. P. Bisen · Nameeta Brahme · Ravi Sharma

Received: 26 January 2014 / Accepted: 7 July 2014 / Published online: 19 August 2014

Abstract $Sr_2MgSi_2O_7:Eu^{2+}$, Dy^{3+} and $Ca_2MgSi_2O_7:Eu^{2+}$, Dy^{3+} phosphors were synthesized by the high-temperature solid-state reaction method. The phase structure of the prepared phosphors was of akermanite type, which belongs to the tetragonal crystallography. The EDX and FTIR spectra confirm the presence of elements in prepared phosphors. $Sr_2MgSi_2O_7:Eu^{2+}$, Dy^{3+} and $Ca_2MgSi_2O_7:Eu^{2+}$, Dy^{3+} phosphors would emit blue and green light; the main emission peaks that appeared at 465 and 535 nm belong to the broad emission band ascribed to the $4f^65d^1 \rightarrow 4f^7$ transition. Decay graph indicates that both the phosphors have fast decay and slow decay. Investigation into afterglow property showed that the $Sr_2MgSi_2O_7:Eu^{2+}$, Dy^{3+} phosphor held better afterglow property than $Ca_2MgSi_2O_7:Eu^{2+}$, Dy^{3+} phosphors. ML measurements showed a linear increase in the ML intensity with the impact velocity of the moving piston.

Keywords $Sr_2MgSi_2O_7:Eu^{2+}$, Dy^{3+} · $Ca_2MgSi_2O_7:Eu^{2+}$, Dy^{3+} · Phosphors · Afterglow · Photoluminescence · Mechanoluminescence

Introduction

Persistent luminescence has been among the most popular subjects of investigations in the storage phosphors field since the late 1990s. Alkaline earth aluminates doped with the Eu^{2+} and R^{3+} ions ($MAl_2O_4:Eu^{2+}$, R^{3+}; M = Ca, Sr; R = Nd, Dy) have

I. P. Sahu · D. P. Bisen · N. Brahme · R. Sharma
School of Studies in Physics & Astrophysics, Pt. Ravishankar Shukla University, Raipur 492010, Chhattisgarh, India
e-mail: dpbisen@rediffmail.com

R. Sharma (✉)
Govt. Arts and Commerce Girls College, Devendra Nagar, Raipur 492001, Chhattisgarh, India
e-mail: rvsharma65@gmail.com

been introduced as new commercial persistent luminescence materials to replace ZnS:Cu, Co [1–3]. The luminescence properties of the aluminates are degraded when exposed to water and hence their use in luminous paints as a pigment is limited. Generally, in Eu^{2+} and Dy^{3+} co-doped systems, the Eu^{2+} is considered as an activator and the Dy^{3+} to produce some traps for electrons or holes [4, 5]. Recently, great attention has been paid to investigating the compounds of the melilite group. The melilites are a large group of compounds characterized by the general formula $M_2T^1T^2_2X_7$, where M is a large monovalent or divalent cation, T^1 is a small divalent or trivalent cation in tetrahedral, T^2 is also a small cation in the other tetrahedral, and X is an anion. Afterglow in melilite has already been well documented [6–9]. Currently, the ML phenomenon has attracted more attention because of its potential application for sensing structural damage, fractures, and deformation. Many efforts have been devoted for developing ML sensors due to their various applications such as visualization of stress, damage detection for airplanes or cars, and the study of human diseases in the near future. For these ML sensors, development of ML phosphors with various colors has much importance. At the same time, the high stabilities, such as resistance of water and thermal stability, are also very important for the application of ML [10, 11]. In order to search better silicate ML phosphors, we investigated the europium and dysprosium-doped $M_2MgSi_2O_7$:Eu^{2+}, Dy^{3+}; M = Sr, Ca for different color and intensity [12]. The $Sr_2MgSi_2O_7$:Eu^{2+},Dy^{3+} and $Ca_2MgSi_2O_7$:Eu^{2+},Dy^{3+} phosphors were prepared by the high-temperature solid-state reaction method under a weak reducing atmosphere. This paper reports the structural characterization on the basis of XRD, EDX, and FTIR. The photoluminescence, mechanoluminescence, and afterglow properties were also studied.

Experimental

Sample preparation

The powder samples of $Sr_2MgSi_2O_7$:Eu^{2+}, Dy^{3+} (SMSED) and $Ca_2MgSi_2O_7$:Eu^{2+}, Dy^{3+} (CMSED) were prepared by solid-state reaction method. The raw materials are $SrCO_3$ (99.90 %), $CaCO_3$ (99.90 %), MgO (99.90 %), SiO_2 (99.99 %), Eu_2O_3 (99.99 %), and Dy_2O_3 (99.99 %), all of analytical purity, were employed in this experiment. Boric acid [H_3BO_3 (99.90 %)] was added as a flux. Initially, the raw materials were weighed according to the nominal compositions of $Sr_2MgSi_2O_7$:Eu^{2+}, Dy^{3+} and $Ca_2MgSi_2O_7$:Eu^{2+}, Dy^{3+}. Then the powders were mixed and milled thoroughly for 2 h using an agate mortar and pestle. The grinded sample was placed in an alumina crucible and subsequently fired at 1,050 °C for 3 h in a weak reducing atmosphere. The weak reducing atmosphere was generated with the help of activated charcoal.

Characterization

The XRD pattern was obtained from a Bruker D8 Advanced X-ray powder diffractometer using Cu-Kα radiation and the data were collected over the 2θ

range 10–70° at room temperature. The phase structure of the sample was verified with the help of joint committee for powder diffraction studies (JCPDS) file (JCPDS: 75–1736, 87–0046). A Fourier transform infrared (FTIR) spectrum was recorded with the help of IR Prestige-21 by SHIMADZU for investigating the fingerprint region and functional groups on the surface of prepared phosphor. The FTIR spectra were collected in the middle infrared region (400–4,000 cm^{-1}) by mixing the sample with potassium bromide (KBr). The excitation and emission spectra of sintered phosphors were recorded by spectrofluorophotometer (SHIMADZU, RF 5301 PC) using a xenon lamp as an excitation source. The decay curves were recorded with a time-resolved fluorescence spectrophotometer (TRFS). Samples were excited with 340-nm pulse nano LED light. Mechano-luminescence was observed by a homemade laboratory system. All measurements were carried out at room temperature.

Experimental setup for ML

The experimental set up used for the impulsive deformation of ML is shown in Fig. 1. The prepared phosphors were stressed by a dropping load of cylindrical shape (moving piston) of a mass of 400 g. To change the impact force, the load was dropped from different heights. The samples were wrapped in aluminum foil and kept in the dark until the ML studies were carried out. RCA 931A photomultiplier tube was positioned below the Lucite plate and the output was connected to the storage oscilloscope. In Fig. 1, 1-stand; 2-pulley; 3-metallic wire; 4-load; 5-guiding cylinder; 6-aluminium foil; 7-phosphors; 8-transparent Lucite plate; 9-wooden block; 10-photomultiplier tube (PMT); 11-oscilloscope; 12-iron base mounted on a table.

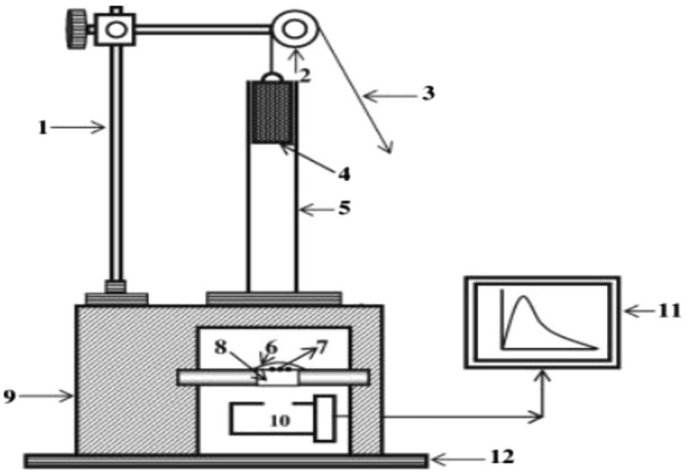

Fig. 1 Schematic diagram of the experimental setup for ML measurement

Results and discussion

XRD analysis

XRD patterns of the $Sr_2MgSi_2O_7:Eu^{2+}$, Dy^{3+} and $Ca_2MgSi_2O_7:Eu^{2+}$, Dy^{3+} phosphors are shown in Fig. 2a and b. The position and intensity of diffraction peaks of $Sr_2MgSi_2O_7:Eu^{2+}$, Dy^{3+} and $Ca_2MgSi_2O_7:Eu^{2+}$, Dy^{3+} were found to be consistent with that of the JCPDS file (JCPDS: 75–1736) and (JCPDS: 87–0046) [13–14]. The result revealed that the phase structure of the $Sr_2MgSi_2O_7:Eu^{2+}$, Dy^{3+} and $Ca_2MgSi_2O_7$: Eu^{2+}, Dy^{3+} phosphors are of akermanite type, which belongs to the tetragonal crystallography with space group $P4\bar{2}_1m$, this structure is a member of the melilite group and forms a layered compound. From the analysis of XRD, it was revealed that no impurity phase has been observed in the compositions, clearly implying that the little amount of doped rare earth ions have almost no effect on the XRD of the prepared phosphors.

Energy-dispersive X-ray spectroscopy (EDX)

The composition of the powder sample was measured using EDX. Table 1 shows the compositional elements of $Sr_2MgSi_2O_7:Eu^{2+}$, Dy^{3+} and $Ca_2MgSi_2O_7:Eu^{2+}$, Dy^{3+}, which is compared with the standard element. Energy-dispersive X-ray spectroscopy (EDX) is a standard procedure for identifying and quantifying elemental composition of sample area as small as a few nanometers. The existence of europium (Eu) and dysprosium (Dy) in the phosphors is clear in their corresponding EDX spectra. There appeared no other emissions apart from Sr, Mg, Si, and O in $Sr_2MgSi_2O_7:Eu^{2+}$, Dy^{3+} and Ca, Mg, Si and O in $Ca_2MgSi_2O_7:Eu^{2+}$, Dy^{3+} the EDX spectra of the samples. In the spectrum, intense peaks are present that confirm the formation of $Sr_2MgSi_2O_7:Eu^{2+}$, Dy^{3+} and $Ca_2MgSi_2O_7:Eu^{2+}$, Dy^{3+} phosphors in Fig. 3a and b, respectively.

Fourier transform infrared spectra (FTIR)

Fourier transform infrared spectroscopy (FTIR) has been widely used for the identification of organic and inorganic compounds. The infrared spectrum of an inorganic compound represents its physical properties. Spectroscopically, the middle infrared region (400–4,000 cm^{-1}) is extremely useful for the study of organic and inorganic compounds. Figure 4a and b shows the FTIR spectra of $Sr_2MgSi_2O_7:Eu^{2+}$, Dy^{3+} and $Ca_2MgSi_2O_7:Eu^{2+}$, Dy^{3+} phosphors. The wave-number 3,429.43 cm^{-1} for $Sr_2MgSi_2O_7:Eu^{2+}$, Dy^{3+} and 3,444.87 cm^{-1} for $CaMgSi_2O_7:Eu^{2+}$, Dy^{3+} arises due to the O–H stretching mode. The O–H group around the 3,400 cm^{-1} in $Sr_2MgSi_2O_7:Eu^{2+}$, Dy^{3+} and $Ca_2MgSi_2O_7:Eu^{2+}$, Dy^{3+} phosphors are might be due to the presence of moisture. The wave-number 1,762.94 cm^{-1} for $Sr_2MgSi_2O_7:Eu^{2+}$, Dy^{3+} and 1779.32 cm^{-1} for $CaMgSi_2O_7:Eu^{2+}$, Dy^{3+} arises due to the stretching of CO_3^{2-}. The CO_3^{2-} modes (asymmetric stretching) around the 1,700 cm^{-1} in $Sr_2MgSi_2O_7:Eu^{2+}$, Dy^{3+} and $Ca_2MgSi_2O_7:Eu^{2+}$, Dy^{3+} phosphors are due to the presence of

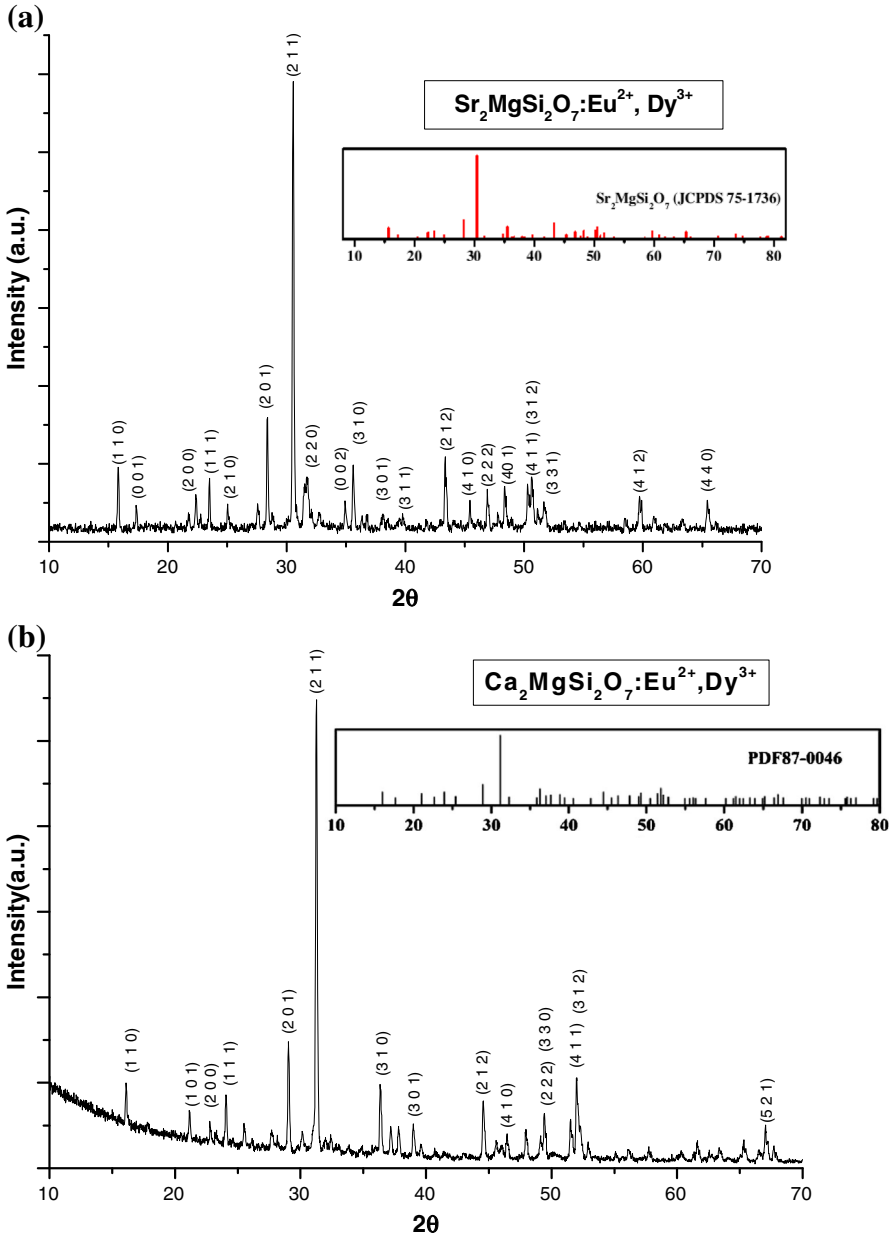

Fig. 2 **a** X-ray diffraction patterns of $Sr_2MgSi_2O_7$: Eu^{2+}, Dy^{3+} phosphor. **b** X-ray diffraction patterns of $Ca_2MgSi_2O_7$: Eu^{2+}, Dy^{3+} phosphor

carbonate. In the experimental section, to prepare the $Sr_2MgSi_2O_7$:Eu^{2+}, Dy^{3+} and $Ca_2MgSi_2O_7$:Eu^{2+}, Dy^{3+} phosphors, we used the raw material ($SrCO_3$, $CaCO_3$) in carbonate form. The free CO_3^{2-} ions have a D3 h symmetry (trigonal planar) and its

Table 1 Composite element of $Sr_2MgSi_2O_7:Eu^{2+}$, Dy^{3+} and $Ca_2MgSi_2O_7:Eu^{2+}$, Dy^{3+}

Composite element of prepared phosphors							
(a) $Sr_2MgSi_2O_7:Eu^{2+}$, Dy^{3+}				(b) $Ca_2MgSi_2O_7:Eu^{2+}$, Dy^{3+}			
Sr. no	Elements	Atomic (%)	Weight (%)	Sr. no	Elements	Atomic (%)	Weight (%)
1	O K	33.91	63.85	1	O K	42.63	63.82
2	Mg K	4.23	5.23	2	Mg K	6.09	6.00
3	Si K	13.54	14.53	3	Si K	14.95	12.75
4	Sr L	47.21	16.18	4	Ca L	26.79	16.01
5	EuL	0.10	0.02	5	EuL	1.18	0.19
6	DyL	1.00	0.18	6	DyL	8.36	1.23
Total		99.99	99.99	Total		99.99	99.99

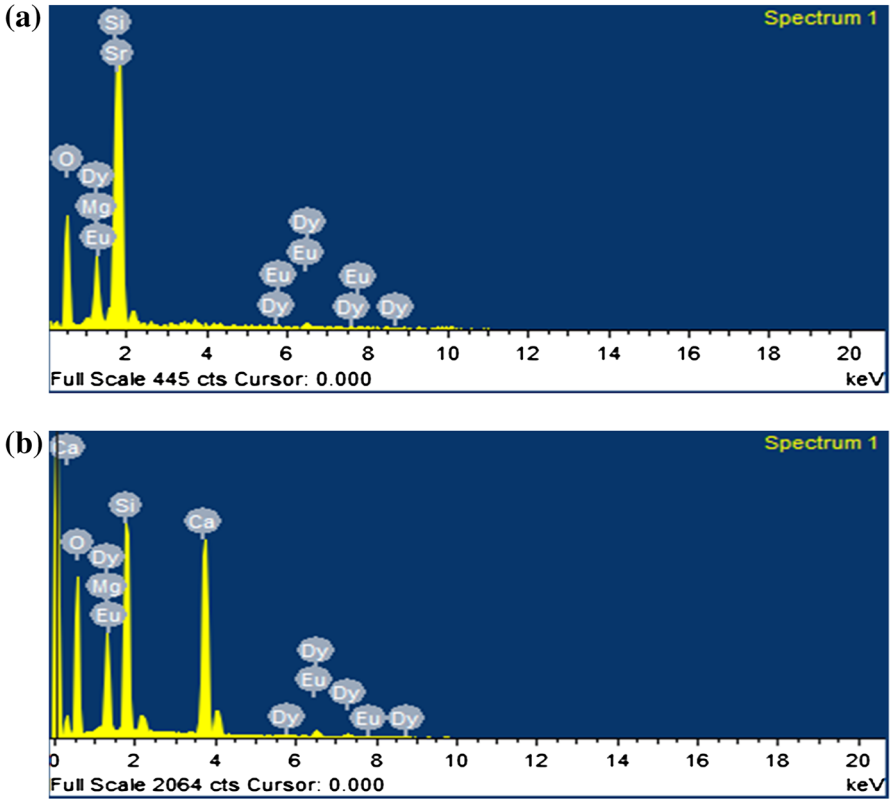

Fig. 3 **a** EDX spectra of $Sr_2MgSi_2O_7$: Eu^{2+}, Dy^{3+} phosphor. **b** EDX spectra of $Ca_2MgSi_2O_7$: Eu^{2+}, Dy^{3+} phosphor

spectrum is dominated by the band at 1,700 cm^{-1}. The vibration bands around 1,643.35 and 1,485.19 cm^{-1} for $Sr_2MgSi_2O_7:Eu^{2+}$, Dy^{3+} are assigned due to the Mg^{2+} and Sr^{2+} and 1,631.78 and 852.54, 740.57 cm^{-1} for $CaMgSi_2O_7:Eu^{2+}$, Dy^{3+}

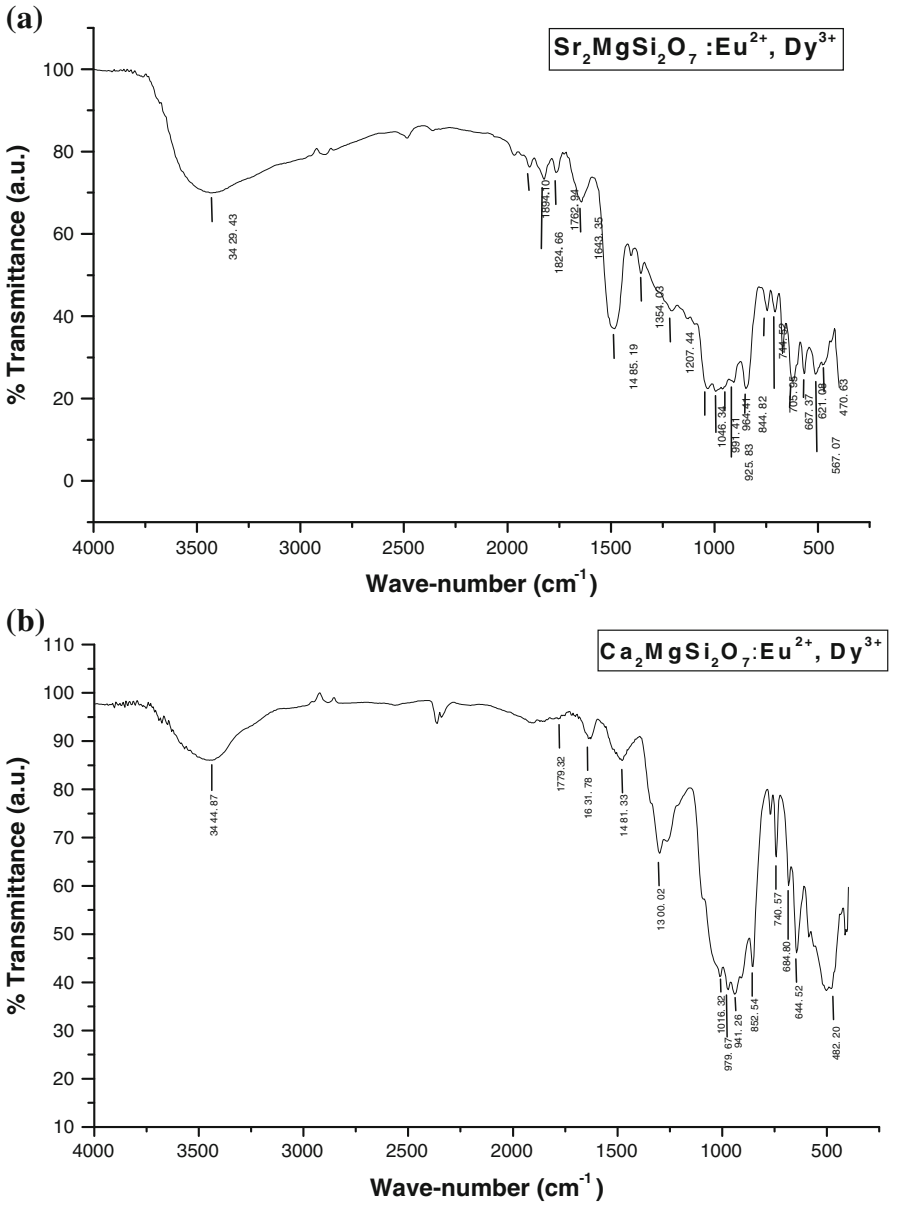

Fig. 4 **a** FTIR spectra of $Sr_2MgSi_2O_7$: Eu^{2+}, Dy^{3+} phosphor. **b** FTIR spectra of $Ca_2MgSi_2O_7$: Eu^{2+}, Dy^{3+} phosphor

are assigned due to the Mg^{2+} and Ca^{2+}. The wave-numbers 1,046.34, 991.41, 964.41, 925.83, and 844.82 cm^{-1} for $Sr_2MgSi_2O_7$:Eu^{2+}, Dy^{3+} and 1,016.32, 979.67, and 941.26 cm^{-1} for $Ca_2MgSi_2O_7$:Eu^{2+}, Dy^{3+} are due to the (Si–O_b–Si) and (Si–O_{nb}) stretching modes. The wave-numbers 744.52, 705.95, 667.37, 621.08, and

567.07 cm^{-1} for $Sr_2MgSi_2O_7:Eu^{2+}$, Dy^{3+} and 684.80, 644.52 cm^{-1} for $Ca_2MgSi_2O_7:Eu^{2+}$, Dy^{3+} arises due to the (Si–O–Si) bending modes and the wave-number 470.63 cm^{-1} for $Sr_2MgSi_2O_7:Eu^{2+}$, Dy^{3+} and 482.20 cm^{-1} for $Ca_2MgSi_2O_7:Eu^{2+}$, Dy^{3+} are based on the (Si–O–Si) bending modes as well as the Mg–O modes. In $Sr_2MgSi_2O_7:Eu^{2+}$, Dy^{3+}; and $Ca_2MgSi_2O_7:Eu^{2+}$, Dy^{3+}; Mg^{2+} occupy the tetrahedral sites. FTIR spectra confirm the component of $Sr_2MgSi_2O_7:Eu^{2+}$, Dy^{3+} and $Ca_2MgSi_2O_7:Eu^{2+}$, Dy^{3+} phosphors [15–21].

Photoluminescence (PL)

The excitation and emission spectra of $Sr_2MgSi_2O_7:Eu^{2+}$, Dy^{3+} and $Ca_2MgSi_2O_7:Eu^{2+}$, Dy^{3+} phosphors are shown in Fig. 5a and b. The excitation spectra were observed in the range of 200–425 nm and emission spectra were recorded in the range of 400–650 nm. The results illustrate that both of them are broadband spectra.

The excitation broadband is due to transitions of ($4f^7$) ground state to excited state ($4f^65d^1$) [$4f^7 \rightarrow 4f^65d^1$] and emission broadband is due to transitions of excited state ($4f^65d^1$) to ground state ($4f^7$) [$4f^65d^1 \rightarrow 4f^7$]. In Fig. 5a, there are four excitation peaks found at 269, 278, 335, and 353 nm and corresponding to emission peaks that occurred at 465 nm, which emit blue color. Similarly, in Fig. 5b there are four excitation peaks found at 270, 279, 315, and 340 nm, and corresponding emission peaks were recorded at 535 nm, which emits green color.

In Fig. 5a and b, the main emission peak at 465 nm and 535 nm is ascribed to the $4f^65d^1 \rightarrow 4f^7$ transition of Eu^{2+}, but there is no special emission of Dy^{3+} and Eu^{3+} ions in the spectra, which implies that Eu^{3+} ions have been reduced to Eu^{2+} completely, and the co-doped Dy^{3+} did not emit any color and transferred the absorbed energy to Eu^{2+} ions in the $Sr_2MgSi_2O_7:Eu^{2+}$, Dy^{3+} and $Ca_2MgSi_2O_7:Eu^{2+}$, Dy^{3+} crystal lattice. The co-doped Dy^{3+} plays a role as a hole-trapped center at the hole trap levels, which capture the free electrons or holes when Eu^{2+} is excited and then release the free electrons to the conduction band. It is known that the blue emission that peaked at 465 nm corresponds to the transitions of $^4F_{9/2} \rightarrow {}^6H_{15/2}$, and 535 nm corresponds to the transitions of $^4F_{9/2} \rightarrow {}^6H_{13/2}$ this emission belongs to hypersensitive transition, which strongly depends on outside environments of Dy^{3+} ions.

Decay

Figure 6 shows the typical decay curves of $Sr_2MgSi_2O_7:Eu^{2+}$, Dy^{3+} and $Ca_2MgSi_2O_7:Eu^{2+}$, Dy^{3+} phosphors. The initial afterglow intensity of both the material was high. The decay times of phosphors can be calculated by a curve-fitting technique, and the decay curves fitted by the sum of two exponential components have different decay times.

$$I = A_1\exp(-t/\tau_1) + A_2\exp(-t/\tau_2), \quad (1)$$

where I is phosphorescence intensity, A_1, A_2 are constants, t is time, τ_1, and τ_2 are decay times (in nanoseconds) for the exponential components. Decay curves are

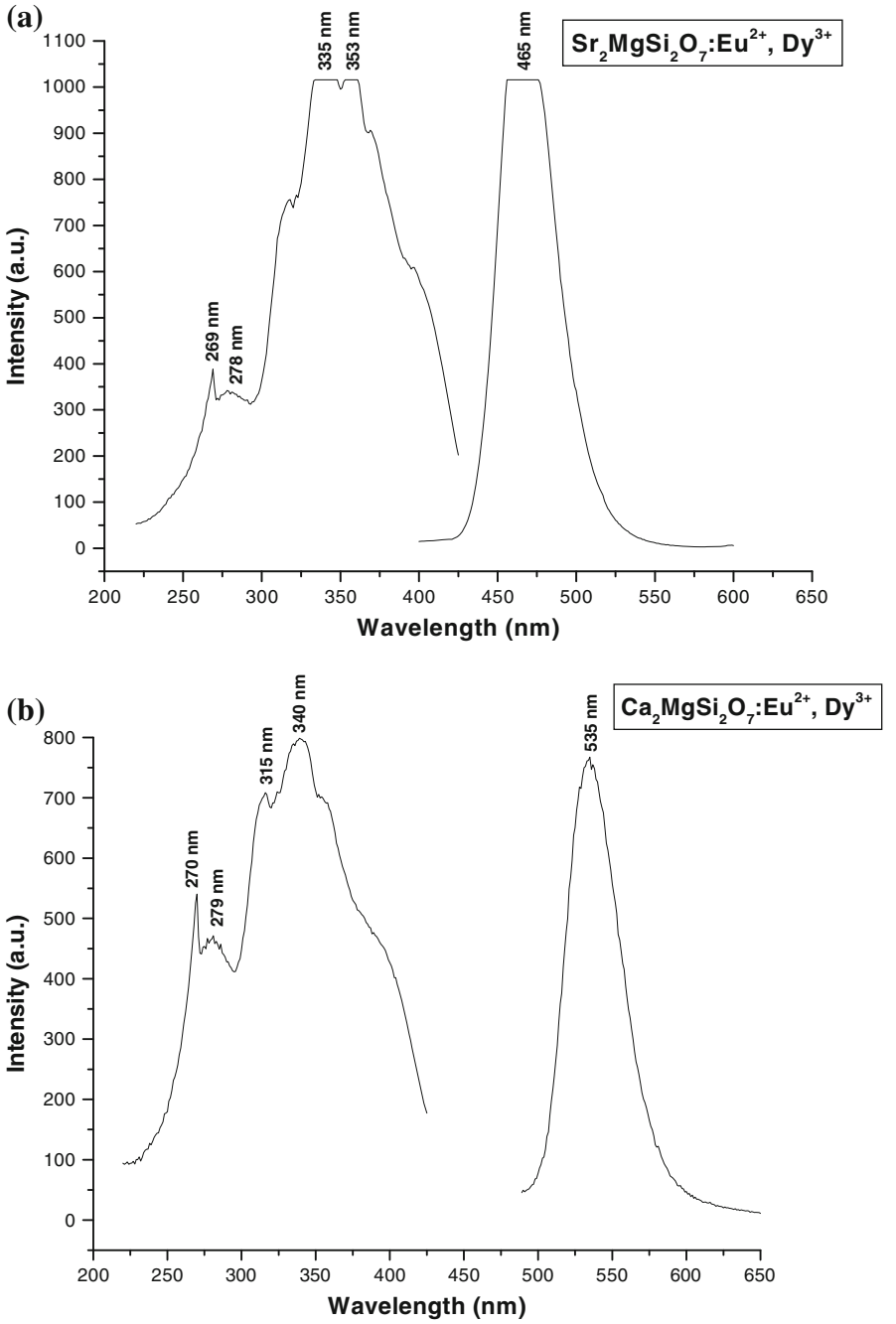

Fig. 5 **a** Excitation and emission spectra of $Sr_2MgSi_2O_7:Eu^{2+}$, Dy^{3+} phosphor. **b** Excitation and emission spectra of $Ca_2MgSi_2O_7:Eu^{2+}$, Dy^{3+} phosphor

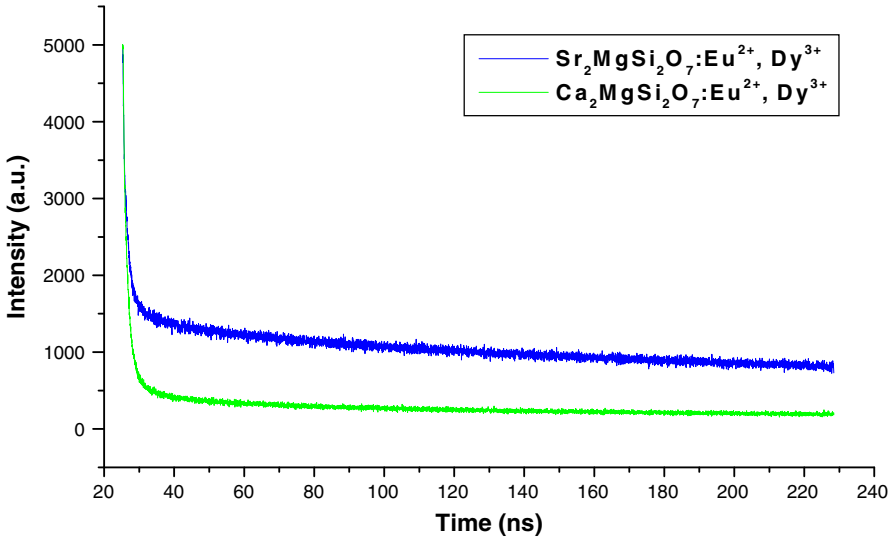

Fig. 6 Decay curves of $Sr_2MgSi_2O_7:Eu^{2+}$, Dy^{3+} and $Ca_2MgSi_2O_7:Eu^{2+}$, Dy^{3+} phosphors

Table 2 Fitting results of the decay curves

Phosphors	τ_1 (ns)	τ_2 (ns)
$Sr_2MgSi_2O_7:Eu^{2+}$, Dy^{3+}	1.35915	89.53232
$Ca_2MgSi_2O_7:Eu^{2+}$, Dy^{3+}	1.29830	42.64905

successfully fitted by Eq. (1) and the fitting curve results are shown in Table 2. Dy^{3+} ions have often been used as co-dopant in the previously developed long afterglow materials (e.g., $SrAl_2O_4:Eu^{2+}$, Dy^{3+}). Alkaline earth ion sites are a very probable source of electron trap [22]. In the alkaline earth silicate, most of the excitation energy will be transferred from the host (from $Dy^{3+} \rightarrow$ to $Eu^{2+} \rightarrow$ to host).

However, part of the excitation energy will be stored when some of the excited carriers drop into the traps, instead of returning to the ground states. Later, the traps created by Dy^{3+} are deeper than those created by Eu^{2+} and with thermal excitation at proper temperature; these carriers will be released from the traps and transferred via the host to the Dy^{3+} ions, followed by the characteristic Dy^{3+} emissions as long afterglow. Dy^{3+} in the silicates act as traps, meanwhile Dy^{3+} can also act as luminescent centers, thus the persistence time is prolonged [22].

Mechanoluminescence (ML)

Figure 7a and b shows the characteristic curve between ML intensity versus time for different heights on $Sr_2MgSi_2O_7:Eu^{2+}$, Dy^{3+} and $Ca_2MgSi_2O_7:Eu^{2+}$, Dy^{3+}

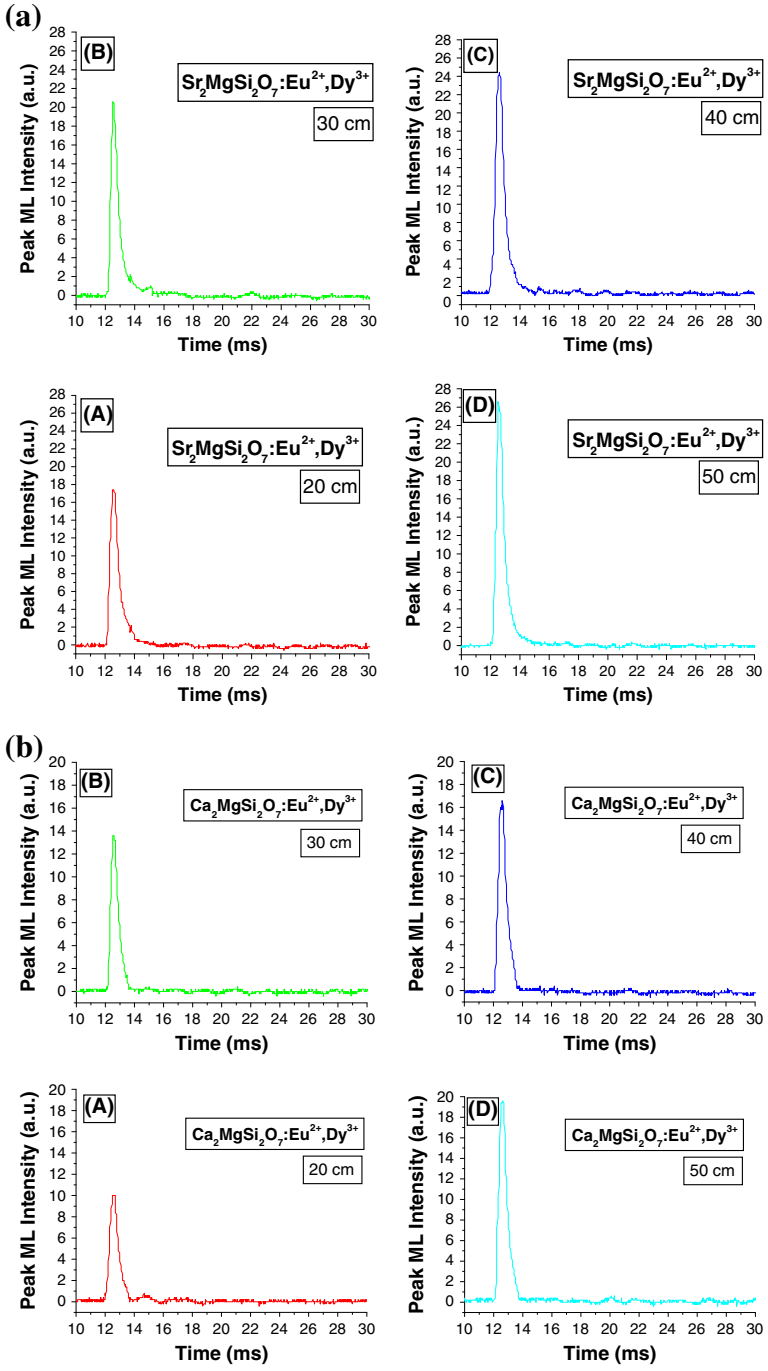

Fig. 7 **a** ML intensity versus time of $Sr_2MgSi_2O_7:Eu^{2+}$, Dy^{3+} phosphor. **b** ML intensity versus time of $Ca_2MgSi_2O_7:Eu^{2+}$, Dy^{3+} phosphor

phosphors. The experiment was carried out for a fixed mass (400 g). The quantity of the sample was kept the same for all the cases. The figure A, B, C, and D shows ML curves dropped from different heights 20, 30, 40, and 50 cm, respectively. These figures showed that the ML intensity increases linearly with increases in the falling height of the moving piston; that is, the ML intensity depending upon the impact velocity. The maximum ML intensity has been obtained for the 50-cm dropping height (for both $Sr_2MgSi_2O_7$:Eu^{2+}, Dy^{3+} and $Ca_2MgSi_2O_7$:Eu^{2+}, Dy^{3+}). The synthesized phosphors were not irradiated by any of the excitation source such as ultra-violet, laser, X-ray, β-rays, or γ-rays.

Figure 8a and b shows the characteristics curve between peak ML intensity versus impact velocity of $Sr_2MgSi_2O_7$:Eu^{2+}, Dy^{3+} and $Ca_2MgSi_2O_7$:Eu^{2+}, Dy^{3+} phosphors. The strait line found implies that the ML intensity increases linearly with the increasing impact velocity [$\sqrt{2gh}$ {where h is the different heights of moving piston (20, 30, 40, 50 cm)}]. It can also be said that ML intensity increases with increasing mechanical stress. When the moving piston hits the prepared sample, it produces a piezoelectric field in the prepared phosphors as they are non-centrosymmetric. The piezoelectric field near certain defect centers may be high due to the change in the local structure. The piezoelectric field reduces the trap depth of the carriers. The decrease in trap depth causes a transfer of electrons from electron traps to the conduction band. Subsequently, the moving electrons in the conduction band are captured in the excited state, located at the bottom of the conduction band, whereby excited ions are produced. The subsequent recombination of electrons with the hole centers gives rise to the light emission [23, 24]. It was found that ML emission was observed even when the height of the moving piston was comparatively low (10 cm).

Figure 9a and b shows the ML spectrum of $Sr_2MgSi_2O_7$:Eu^{2+}, Dy^{3+} and $Ca_2MgSi_2O_7$:Eu^{2+}, Dy^{3+} phosphors. The spectrum consists of a broad emission band peaking at 460 and 530 nm, which is similar to the spectra of PL spectrum of $Sr_2MgSi_2O_7$:Eu^{2+}, Dy^{3+} and $Ca_2MgSi_2O_7$:Eu^{2+}, Dy^{3+} phosphors. The small difference of the peak location between the ML (460 nm for $Sr_2MgSi_2O_7$:Eu^{2+}, Dy^{3+} and 530 nm for $Ca_2MgSi_2O_7$:Eu^{2+}, Dy^{3+}) and PL (465 and 535 nm) can be ascribed to the different measurement devices. This implies that ML is emitted from the same emitting center of Eu^{2+} ions as PL, which is also produced by the transition of Eu^{2+} ions between the ($4f^6 5d^{1)}$ excited state to ($4f^7$) ground state. Furthermore, both prepared phosphors have a tetragonal structure with space group $P\bar{4}2_1mm$; previous research has revealed that the crystal with these structure possesses piezo-electrification. When a mechanical stress, such as compress, friction, and striking, and so on, was applied on the (for both $Sr_2MgSi_2O_7$:Eu^{2+}, Dy^{3+} and $Ca_2MgSi_2O_7$:Eu^{2+}, Dy^{3+}) phosphor, a piezoelectric field can be produced. The strain energy impels the filled shallow trap to release holes to the valence band. Then, free holes excite Eu^{+} to produce Eu^{2+}, which returns to the ($4f^7$) ground state by emitting light. Based on the above analysis, these phosphors can be used as sensors to detect the stress on an object [25–29].

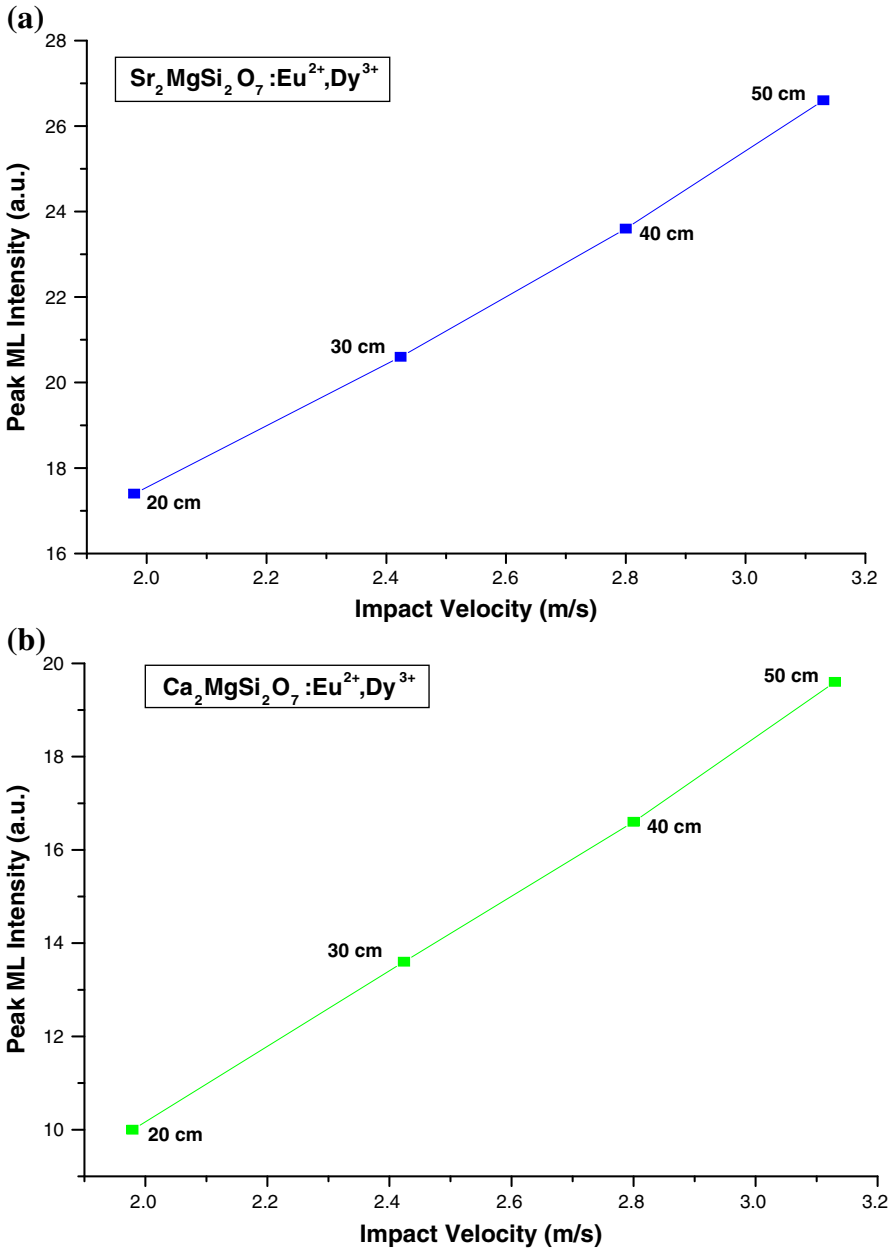

Fig. 8 **a** Peak ML intensity versus impact velocity of $Sr_2MgSi_2O_7:Eu^{2+}$, Dy^{3+} phosphor. **b** Peak ML intensity versus impact velocity of $Ca_2MgSi_2O_7:Eu^{2+}$, Dy^{3+} phosphor

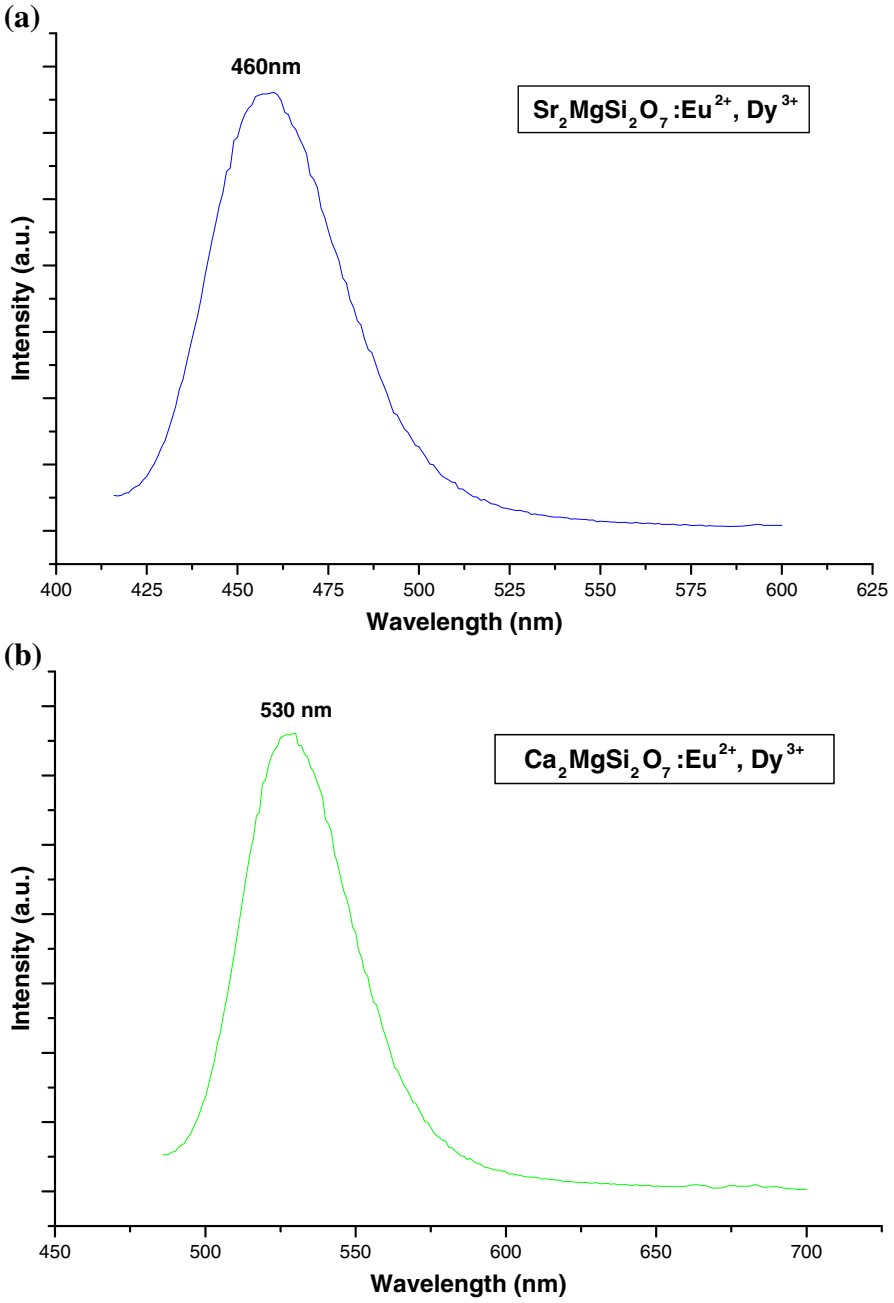

Fig. 9 **a** ML spectra of $Sr_2MgSi_2O_7:Eu^{2+}$, Dy^{3+} phosphor. **b** ML Spectra of $Ca_2MgSi_2O_7:Eu^{2+}$, Dy^{3+} phosphor

Conclusions

$Sr_2MgSi_2O_7:Eu^{2+}$, Dy^{3+} and $Ca_2MgSi_2O_7:Eu^{2+}$, Dy^{3+} phosphors with a long afterglow were synthesized by the high-temperature solid-state reaction method under weak reducing atmospheres. The radius of Eu^{2+} (1.12 Å) and Dy^{3+} (0.99 Å) is very close to that of Sr^{2+} (about 1.12 Å), Ca^{2+} (about 1.12 Å) rather than Mg^{2+} (0.65 Å) and Si^{4+} (0.41 Å) nm). Therefore, the Eu^{2+} and Dy^{3+} ions are expected to occupy the Sr^{2+} sites in $Sr_2MgSi_2O_7$ and Ca^{2+} sites in $Ca_2MgSi_2O_7$ host. The EDX and FTIR spectra confirm the present elements in $Sr_2MgSi_2O_7:Eu^{2+}$, Dy^{3+} and $Ca_2MgSi_2O_7:Eu^{2+}$, Dy^{3+} phosphors. The emission peaks of $Ca_2MgSi_2O_7:Eu^{2+}$, Dy^{3+} phosphor, when compared with that of $Sr_2MgSi_2O_7:Eu^{2+}$, Dy^{3+} phosphor, shift towards the longer wavelength direction, which can be explained by the slight difference in the crystal structure. The mechanoluminescence intensity increases linearly with the load and linear relationship has been obtained with the impact velocity, which suggests that both prepared phosphors can be used as sensors to detect the stress on an object.

Acknowledgments We are very much grateful to UGC-DAE Consortium for Scientific Research, Indore (M.P.) for the XRD characterization and we are also very much thankful to Dr. Mukul Gupta for his co-operation. We are very thankful to Dr. K.V.R. Murthy, Department of Applied physics, M.S. University Baroda for the Photoluminescence Study.

References

1. Y. Chen, B. Liu, M. Kirm, Z. Qi, C. Shi, M. True, S. Vielhauer, G. Zimmerer, J. Lumin. **118**, 70–78 (2006)
2. W. Pan, G. Ning, X. Zhang, J. Wang, Y. Lin, J. Ye, J. Lumin. **128**, 1975–1979 (2008)
3. Hu Yihua, Wu Haoyi, Yinhai Wang, Fu Chujun, Mater. Sci. Eng. B **172**, 276–282 (2010)
4. Y. Lin, Z. Zhang, Z. Tang, X. Wang, J. Zhang, Z. Zheng, J. Eur. Ceram. Soc. **21**, 683 (2001)
5. B. Liu, C. Shi, M. Yin, L. Dong, Z. Xiao, J. Alloys Compd. **387**, 65–69 (2005)
6. C. Shi, Y. Fu, B. Liu, G. Zhang, Y. Chen, Z. Qi, X. Luo, J. Lumin. **122–123**, 11–13 (2007)
7. Y. Murayama, N. Takeuchi, Y. Aoki, T. Matsuzawa, U.S. Patent 5,424,006, 13 June 1995
8. Yu. Gong, Yuhua Wang, Ziqiang Jiang, Xuhui Xu, Yanqin Li, Mater. Res. Bull. **44**, 1916–1919 (2009)
9. N. Kodama, N. Sasakki, M. Yamaga, Y. Masui, J. Lumin. **94**(95), 19–22 (2001)
10. C.N. Xu, T. Watanabe, M. Akiyama, X.G. Zheng, Appl. Phys. Lett. **74**, 2414 (1999)
11. C.N. Xu, T. Wantanabe, M. Akiyama, X.G. Zheng, Appl. Phys. Lett. **74**, 1236 (1999)
12. Y. Gong, Y. Wang, Z. Jiang, X. Xu, Y. Li, Mater Res Bull **44**, 1916–1919 (2009).
13. M. Kimata, Z. Kristallogr **163**, 295 (1983). ICDD data No.75–1736
14. G.M. Kuzmicheva, E.V. Zharikov, A.L. Denisov, **40**, 1422 (1995). ICDD data No.77–1149
15. R.D. Shannon, Acta Cryst. A **32**, 751 (1976)
16. C. Chang, D. Mao, J. Alloy. Compd. **390**, 134 (2005)
17. R.L. Frost, J.M. Bouzaid, B.J. Reddy, Polyhedron **26**, 2405 (2007)
18. G.T. Chandrappa, S. Ghosh, K.C. Patil, J. Mater. Synth. Process. **7**, 273 (1999)
19. P. Makreski, G. Jovanovski, B. Kaitner, A. Gajovic, T. Biljan, Vib. Spectrosc. **44**, 162 (2007)
20. R. Caracas, X. Gonze, Phys. Rev. B **68**, 184102 (2003)
21. M.A. Salim, R. Hussain, M.S. Abdullah, S. Abdullah, N.S. Alias, S.A. Ahmad Fuzi, M.N. Md Yusuf, K.M. Mahbor, Solid State Sci. Technol. **17**(2), 59–64 (2009)
22. T. Aitasalo, P. Daren, J. Holsa, K. Junger, J.C. Krupa, M. Lastusaari, J. Legendziewicz, J. Niittykoski, W. Strek, J. Solid State Chem. **171**, 114 (2003)
23. B.P. Chandra, V.D. Sonwane, B.K. Haldar, S. Pandey, Opt. Mater. **33**, 444–451 (2011)
24. P. Jha, B.P. Chandra, J. Lumin. **143**, 280–287 (2013)

25. H. Zhang, H. Yamada, N. Terasaki, C.-N. Xu, Jpn. J. Appl. Phys. **48**, 04C109 (2009)
26. H. Zhang, H. Yamada, N. Terasaki, C.-N. Xu, Electrochemical and Solid State Letters **10**(10), J129–J131 (2007)
27. H. Zhang, H. Yamada, N. Terasaki, C.-N. Xu, Thin Solid Films **518**, 610–613 (2009)
28. H. Zhang, N. Terasaki, H. Yamada, C.-N. Xu, Int. J. Mod. Phys. B **23**(6 & 7), 1028–1033 (2009)
29. H. Zhang, C.-N. Xu, N. Terasaki, H. Yamada, Phys. E **42**, 2872–2875 (2010)